Collective mode properties in a paired fullerene-ion plasma

W. Oohara,* Y. Kuwabara, and R. Hatakeyama
Department of Electronic Engineering, Tohoku University, Sendai 980-8579, Japan
(Received 25 September 2006; revised manuscript received 12 March 2007; published 9 May 2007)

A pair-ion plasma without electrons consisting of C_{60}^{+} and C_{60}^{-} is generated through the processes of electron-impact ionization, electron attachment, and magnetic filtering. Properties of electrostatic modes propagating along magnetic-field lines are experimentally investigated by externally exciting them with two types of electrodes. It is found that four kinds of wave modes exist and a frequency spectrum of phase lag between the density fluctuations of C_{60}^{+} and C_{60}^{-} is unique in comparison with ordinary electron-ion plasmas. One of the modes is an ion acoustic wave which is divided into two branches at around the ion cyclotron frequency in the presence of a backwardlike mode joining them. The phase lag of the ion acoustic wave strongly depends on the frequency, while those for the other ion plasma and intermediate-frequency waves are constant at π independent of the frequency.

DOI: 10.1103/PhysRevE.75.056403 PACS number(s): 52.27.Ep, 52.35.Fp, 81.05.Tp

I. INTRODUCTION

A typical plasma consists of electrons and positive ions, and an asymmetric diversity of collective plasma phenomena is caused by their large mass difference. On the contrary, pair plasmas consisting of only positive- and negative-charged particles of equal mass have attracted special attention. Such pair plasmas maintain space-time symmetry because the mobility of the particles in electromagnetic fields is the same. Positrons have been spotlighted in connection with antimatter property, e.g., CPT invariance, in high-energy physics and astrophysics, and the pair plasmas consisting of positrons and electrons have been investigated theoretically [1–17]. Both the relativistic and nonrelativistic pair plasmas have been gradually revealed to represent a new state of matter with unique thermodynamic properties drastically different from those of ordinary electron-ion plasmas. Some theoretical works have already been presented, which concern the elementary properties and linear and nonlinear collective modes in nonrelativistic electron-positron plasmas [4,7,10–12,14,15]. A comprehensive two-fluid model has been developed for collective-mode analyses, based on which longitudinal or transverse electrostatic or electromagnetic modes have been studied, and the experimental identification is desired to be undertaken at present. Plasmas including positrons have been generated experimentally in laboratories [18–28]. In particular, the electron-positron plasma is experimentally generated by injecting a low-energy electron beam into the positron plasma. For long-time-scale plasma physics experiments, it is necessary to meet the condition that the annihilation time scale is many orders of magnitude larger than the plasma period. In order to maintain a steady-state plasma over such long durations the pairs must be created prolifically to balance their short annihilation time scales. Thus, it is not easy to generate and maintain the electron-positron plasma. Here our attention is concentrated on the easy and stable state generation of a pair-ion plasma consisting of positive and negative ions of equal mass and its collective-mode identification.

According to our previous work on the generation of an alkali-fullerene plasma (K^{+}, e^{-}, C_{60}^{-}) by introducing a fullerene into a potassium plasma [29–32], fullerenes are candidates for the ion source to realize the pair-ion plasma, because the interaction of electrons with the fullerenes leads to the production of both negative [33–38] and positive [39–43] ions. We have developed a method for generating a pair-ion plasma that consists of only positive and negative ions of equal mass using fullerene [44–47]. Without interruption the pair-ion plasma source has so far been improved drastically in order to increase the plasma density and excite the collective modes.

II. GENERATION OF PAIR-ION PLASMA

The attachment cross-section function for the production of C_{60}^{-} has been determined as a function of electron energy [33–38]. Free-electron attachment occurs over a very broad-energy range, extending to 12 eV. The attachment cross-section curve for such reaction that $C_{60}+e^{-}\rightarrow C_{60}^{-}$, $\sigma(C_{60}^{-})$, exhibits a distinct low-energy threshold ($\sim$0.15 eV). The cross-section value is $\sigma(C_{60}^{-})=100\times10^{-24}$ cm^2 at 0.5 eV. Superimposed on the broad cross section, several resonance structures exist at energies near 1.5, 4.5, 5.5, and 8.0 eV. On the other hand, the ionization cross-section curve for such reaction that $C_{60}+e^{-}\rightarrow C_{60}^{+}+2e^{-}$, $\sigma(C_{60}^{+})$, does not show any precipitous structure, but exhibits a smooth shape in the vicinity of the 50 eV peak [39–43]. The cross-section value is $\sigma(C_{60}^{+})=25\times10^{-24}$ cm^2 at 100 eV. The electron-impact ionization of C_{60} gives rise to a variety of different ions, including stable parent ions, stable fragment ions, and metastable parent or fragment ions. The electron energy dependence of the production of singly and multiply charged parent or fragment ions has been investigated. The cross-section ratios to $\sigma(C_{60}^{+})$ are $\sigma(C_{60}^{2+})/\sigma(C_{60}^{+})\simeq0.22$, $\sigma(C_{60}^{3+})/\sigma(C_{60}^{+})\simeq0.014$, $\sigma(C_{58}^{+})/\sigma(C_{60}^{+})\simeq0.02$, and $\sigma(C_{56}^{+})/\sigma(C_{60}^{+})\simeq0.018$ at 100 eV.

A pair-ion plasma source with fullerene ion species consists of an electron-beam gun, an ion production cylinder,

*Electronic address: oohara@ecei.tohoku.ac.jp

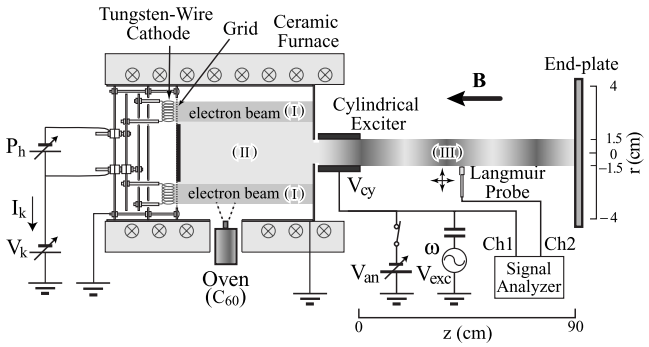

FIG. 1. Schematic drawing of experimental setup. Longitudinal-electrostatic wave modes propagating along *B*-field lines are excited by a cylindrical exciter. Region (I) is the hollow electron-beam part, region (II) is the magnetic filtering part, and region (III) is the experimental part.

and a magnetic filter [44–47]. The electron-beam gun is set inside the ion production cylinder (8 cm diam and 30 cm length) with a thin annulus (inner diameter 3 cm and 0.1 cm thickness) made of copper. The plasma source is installed in a grounded vacuum chamber of 15.7 cm diam and 260 cm length, as shown schematically in Fig. 1. A uniform magnetic field of $B=0.2$ T is applied using solenoid coils and the background gas pressure is 2×10^{-4} Pa. A tungsten wire cathode with a ring structure of 5 cm diam is divided into four parts that are connected in parallel and resistively heated to over 2000 °C. The wire cathode is biased at voltage V_k (<0 V) with respect to a grounded grid anode set at less than 0.5 cm in front of the cathode. A stainless-steel disk of 4 cm diam is concentrically welded onto the grid anode. Thermally emitted low-energy electrons (~0.2 eV) are accelerated by the electric field between the cathode and the anode, and form a hollow electron beam. The cylinder and the annulus are grounded, and the beam flows along the magnetic (B) field lines and is terminated at the annulus. The beam energy E_e can be controlled in the range of 0–150 eV by changing V_k. The cylinder has a hole (3 cm diam) on the sidewall at which an oven for fullerene sublimation is set. A fullerene sample, which is commercially available C_{60} powder of 99.5% purity, is heated in the oven. Typical oven temperatures under operating conditions range between 400 and 600 °C. As a result of sublimation, the fullerene vapor is produced enough to fill the cylinder. The cylinder is fixed inside a cylindrical ceramic furnace and heated to 500 °C. The fullerene vapor is adhered and a solid film is formed on surrounding solid surfaces with less than 350 °C. Thus, the cylinder and the annulus are substantially heated to 500 °C to avoid the adhesion. The cylinder, the annulus, and the oven are made of copper, because the heat conductivity of copper is high (381 $W\,m^{-1}\,K^{-1}$ at 300 °C) and fullerenes (carbon) do not react chemically with copper. The heated cylinder is called a resublimation cylinder, and the introduced fullerene vapor is effectively confined inside the cylinder without the adhesion. The electron beam with a annular cross section collides with neutral C_{60}, and C_{60}^+ is produced by impact ionization. Then low-energy electrons are simultaneously produced and they contribute to producing negative ions. Negative ions produced by electron attachment are singly charged, and the process is simple compared with impact ionization. To produce C_{60}^+ and C_{60}^- concurrently, it is essential that C_{60} has the feature of electron attachment over a broad-energy range. In our previous work [44], a ceramic (LaB_6) plate was used as a cathode. When the LaB_6 cathode is exposed to the fullerene vapor, it is experimentally found that the surface density of thermal electrons emitted on the LaB_6-cathode surface drastically decreases, the same as a barium oxide (BaO) cathode, although the LaB_6 cathode was kept off from the cylinder in order to inhibit the considerable decline of the surface density. In addition, the fullerene vapor was not well confined in the cylinder. The drastic decrease of the surface density is scarcely caused in the present case of the tungsten-wire cathode. Moreover, the electron gun acts as a cap and also plays a role in preventing the fullerene vapor from being lost because it is installed inside the cylinder [45].

The chamber wall is grounded and an end-plate is maintained at a floating potential. For analytic convenience, the whole space of the plasma is divided into three regions, (I), (II), and (III). The hollow electron-beam region is the fullerene-ion production region and is called region (I). Since charged-particle gyroradii are proportional to the $\sqrt{\text{mass/charge}}$ ratio. The gyroradii of C_{60}^+ and C_{60}^- are larger than those of e^-, C_{60}^{2+}, C_{60}^{3+}, C_{58}^+, C_{56}^+ etc., if their kinetic energies perpendicular to the B-field lines are the same. The gyroradius ratio $\rho_{C_{60}^\pm}/\rho_{e^-}$ is particularly high ($\simeq$1100). A preferential ambipolar diffusion of $C_{60}^\pm$ can take place in the radial (r) direction across the B-field lines due to their large gyroradii, i.e., a magnetic-filtering effect [48]. The multiply charged ions and the fragment ions have lower production rates and their gyroradii are smaller, thus they are separated from $C_{60}^\pm$. Only C_{60}^+ and C_{60}^- are expected to exist in the center of the cylinder, region (II), and the electron-free pair-ion plasma generation occurs here. C_{60}^+ and C_{60}^- flow along the B-field lines and pass through the annular hole toward an experimental region, region (III).

A cylindrical or a grid electrode is set in front of the annular hole between regions (II) and (III). The electrode can be biased at V_{an} superimposed by V_{exc} ($V_{cy}=V_{an}+V_{exc}$), where V_{an} is a dc voltage and V_{exc} is an ac voltage of frequency $\omega/2\pi$. The exit position of the electrode is defined as $z=0$ cm, and the pair-ion plasma is terminated at the end-plate ($z=90$ cm). Plasma parameters in region (III) are measured using Langmuir probes, the collectors of which are surrounded with an insulator of ceramic and thus guarded against direct exposure to C_{60} particles and prevented from being contaminated by C_{60}.

III. EXPERIMENTAL RESULTS

A. Static property of pair-ion plasma

The generation property of the pair-ion plasma is measured at $r=0$ cm and $z=5$ cm for $V_{cy}=0$ V by changing the electron-beam energy E_e, as shown in Fig. 2. I_+ and I_- are Langmuir-probe saturation currents of C_{60}^+ and C_{60}^-, respectively, which are considered to be proportional to the ion

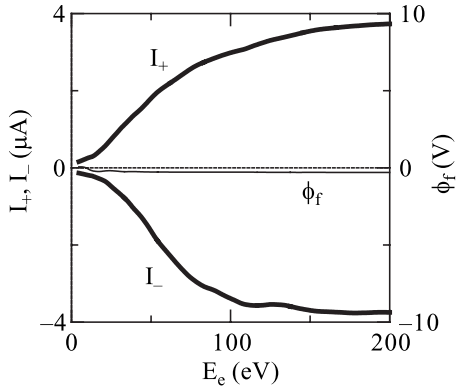

FIG. 2. Generation property of the pair-ion plasma for variations in the electron-beam energy E_e in region (III). Positive and/or negative-saturation currents (I_+, I_-) and floating potential (ϕ_f) of Langmuir probe are measured at $z=5$ cm.

densities. ϕ_f is a floating potential of the probe. When E_e increases from 0 eV, the pair-ion plasma begins to be generated. The plasma density gradually increases and almost saturates at around $E_e=150$ eV. ϕ_f changes depending on E_e in $E_e<50$ eV and attains a saturated value of about −0.3 V for $E_e>50$ eV. The number of C_{60}^- produced is thought to be smaller than that of C_{60}^+ produced in region (I), because a part of low-energy electrons produced in the process of C_{60}^+ production contribute to produce C_{60}^-. But I_+ and I_- are almost the same for the reason of the ambipolar diffusion in the magnetic filter between regions (I) and (II). The symmetry breaking of the saturation currents is sometimes caused for $E_e>150$ eV, since some electrons also diffuse inwardly and exit in region (III). Thus, the measurements of the plasma parameters and the mode propagation are performed at $E_e=100$ eV as follows.

A typical current-voltage (I_p-V_p) characteristic (solid curve) and its differential curve (dI_p/dV_p, dashed curve) are shown in Fig. 3 for $V_{cy}=0$ V and $E_e=100$ eV. The I_p-V_p characteristic is almost symmetrical, and V_p yielding a peak of the differential curve indicates the plasma potential and almost coincides with the floating potential $\phi_f=-0.3$ V. The plasma and floating potentials are close to 0 V which is almost equal to the potential of the grid and the annulus. The static potential structures including sheaths is found not to be formed in the pair-ion plasma because the mobilities of the ions are almost the same. The plasma density and the ion temperatures are calculated from the probe characteristics. The density is $1-2\times10^8$ cm^{-3} at $E_e=100$ eV, while the temperatures of C_{60}^+ and C_{60}^-, T_+ and T_-, are 0.3–0.5 eV. Strictly speaking, T_+ is slightly different from T_- since the charged process is physically different between positive and negative ions.

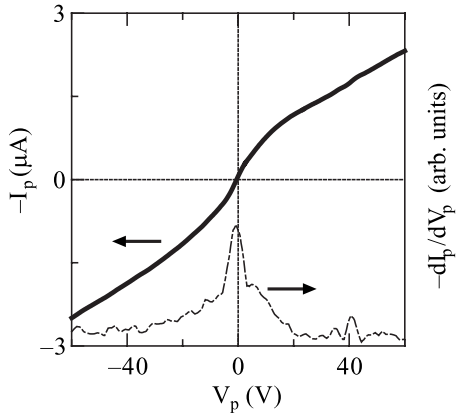

FIG. 3. Typical current-voltage (I_p-V_p, solid curve) and differentiated (dI_p/dV_p, dashed curve) characteristics of the probe measured at $E_e=100$ eV.

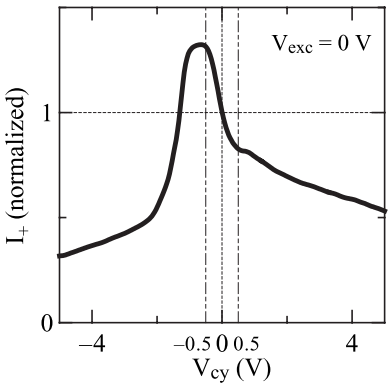

FIG. 4. Positive-saturation current I_+ as a function of dc bias voltage V_{cy} of the cylindrical electrode set between regions (II) and (III), where $V_{cy}=V_{an}$ and $V_{exc}=0$. I_+ is normalized by I_+ at $V_{cy}=0$ V.

The probe characteristic shows a linear change in $|V_p|>20$ V. In general, the saturation currents of the probe indicate the currents which do not almost change for variations in $|V_p|$, but $|I_p|$ is considered to linearly increase with increasing $|V_p|$ in not only the pair-ion plasma but also ionic plasmas without electrons. The shielding is insufficient in the ionic plasmas, a particle-capture radius of the probe largely increases, and $|I_p|$ also increases with increasing $|V_p|$.

Here, the cylindrical electrode set in front of the annular hole between regions (II) and (III) is time independently biased at V_{cy} ($=V_{an}$, $V_{exc}=0$ V). Figure 4 gives the plasma density as a function of V_{cy} at $r=0$ cm and $z=5$ cm for $E_e=100$ eV, where I_+ is normalized by I_+ at $V_{cy}=0$ V. The normalized I_+ is 1.31 and 0.82 at $V_{cy}=-0.5$ V and +0.5 V, respectively. Thus, the plasma density can be modulated by temporally changing V_{cy} ($V_{exc}\neq0$), and longitudinal-electrostatic modes can be excited in region (III). In the present situation it is extremely difficult to excite electromagnetic modes relevant to the plasma because the density and the temperature are relatively low and the induction current of the ions is very small.

B. Dynamic property of pair-ion plasma

Longitudinal-electrostatic modes are excited in region (III) by the cylindrical exciter [44–46]. Figure 5 gives typical Lissajous curves of V_{cy} and I_+ at $\omega/2\pi=7$, 12, and 36 kHz, where I_+ is normalized by the time-averaged component $\bar{I}_+$ and measured at $z=5$ cm under the condition that the switch of V_{an} is cut, i.e., $V_{cy}=V_{exc}$. The damping of the excited modes as they propagate depends on the frequency. Thus, the

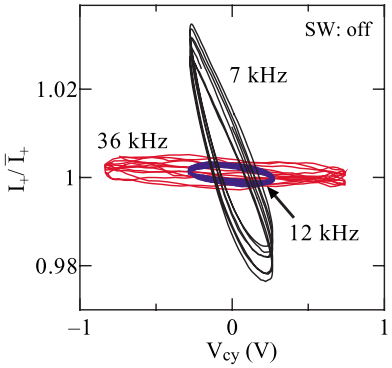

FIG. 5. (Color online) Typical Lissajous curves of V_{cy} and I_+ at $\omega/2\pi=7$, 12, and 36 kHz, where I_+ is normalized by the time-averaged component $\bar{I}_+$ and $V_{cy}=V_{exc}$.

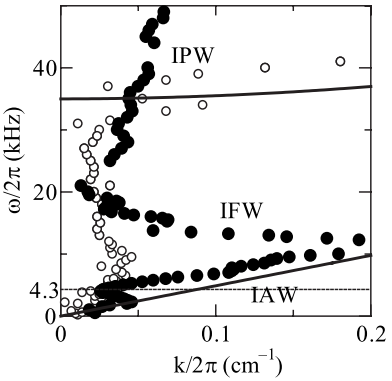

FIG. 6. Dispersion relations of electrostatic modes propagating along B-field lines. Closed circles denote the dispersion relations measured at $r=0$ cm, $z=4-6$ cm, $E_e=100$ eV, and $B=0.2$ T. Solid curves are the calculated dispersion curves mentioned in Sec. IV. The ion cyclotron frequency of C_{60} ions is 4.3 kHz indicated by the dashed line. For comparison, the previous results are also shown by open circles.

propagating-mode amplitude does not exactly correspond to the excited-mode amplitude right after the excitation, while the Lissajous curves qualitatively indicate the relation between V_{cy} and the excited-mode amplitude. The peak to peak amplitude of $I_+/\bar{I}_+$ at $\omega/2\pi=7$ kHz is about 0.06 and relatively large at the peak to peak voltage amplitude $V_{cy}=0.5$ V. In the case of dc-voltage application, the change of $I_+/\bar{I}_+$ becomes about 0.49 at the corresponding change of V_{cy} (=0.5 V) as mentioned in Sec. III A. On the contrary, the amplitude at $\omega/2\pi=12$ kHz is small $I_+/\bar{I}_+\sim 0.005$ even though V_{cy} is the same value of 0.5 V. $I_+/\bar{I}_+$ at $\omega/2\pi=36$ kHz is about 0.006 at $V_{cy}=1.6$ V, and the mode itself is hard to be excited, because the response speed of the ions is low and the ions are difficult to follow such a high-frequency voltage variation. Therefore V_{cy} must be small in the low-frequency range and large in the high-frequency range in order to maintain constant mode amplitude in the plasma for a variety of frequencies. Here, since the purpose for exciting the modes is to investigate the linear property, the large amplitude and nonlinear excitations of the modes are undesirable. As a result of a series of measurements, the suitable amplitude for linear excitation is found to depend on the excitation frequency.

The properties of mode propagation along the B-field lines are measured at $r=0$ cm, $z=4-6$ cm, and $E_e=100$ eV. The fluctuation signals are analyzed by YOKOGAWA Electric Corporation SA2400 [fast Fourier transform (FFT)] analyzer, <400 kHz). Channel 1 (Ch1) of the signal analyzer measures the excited signal at frequency $\omega/2\pi$ and channel 2 (Ch2) measures the fluctuation signal of I_+. The phase delay between Ch1 and Ch2 is measured at each $z=4$, 5, and 6 cm, and the wave number k (wavelength) of the propagating modes is obtained from the averaged phase delay. $\omega/2\pi$ is changed from 0.1 kHz to 50 kHz. The dispersion relation of the propagating modes is shown by closed circles in Fig. 6, where solid curves (mentioned in Sec. IV) are the calculated dispersion curves and the dashed line indicates the ion cyclotron frequency $\omega_c/2\pi=4.3$ kHz at $B=0.2$ T. For comparison, the previous results [45,47] are also shown as open circles. There are three modes in the measured dispersion relations, $\omega/2\pi<12$ kHz, $12<\omega/2\pi<20$ kHz, and $\omega/2\pi>20$ kHz, which we refer to as an ion acoustic wave (IAW), an intermediate-frequency wave (IFW), and an ion plasma wave (IPW), respectively. IFW has the feature that the group velocity is negative but the phase velocity is positive, i.e., the mode resembles a backward wave. IAW can be measured in a larger $k/2\pi$ (shorter wavelength) range and IFW is measured more clearly, compared with the previous results [45,47], because the structure of the exciter is improved and the amplitude of V_{cy} is adjusted in accordance with the variation of $\omega/2\pi$. Furthermore, it is definitely shown that IAW divides into two branches at around the ion cyclotron frequency $\omega_c/2\pi=4.3$ kHz. The mode in $2.5<\omega/2\pi<4.3$ kHz is a backwardlike mode and apparently analogous to IFW joining IAW and IPW. The measured dispersion relation of IPW is considerably changed compared with the previous result, the reason for which is not understood at present.

Temporal variations of the positive- and negative-ion densities are measured and compared, the typical results of which are shown in Figs. 7(a)–7(c) for the cases of $\omega/2\pi=0.1$, 10, and 20 kHz, respectively. $\tilde{I}_+$ and $\tilde{I}_-$ indicate the oscillating components of the positive- and negative-saturation currents, corresponding to those of the positive- and negative-ion densities ($\tilde{n}_+$ and $\tilde{n}_-$), measured at $r=0$ cm and $z=5$ cm, respectively. Here, a phase lag φ between the oscillating components $\tilde{I}_+$ and $\tilde{I}_-$ is defined as $\tilde{I}_+=\tilde{I}_-\exp(i\varphi)$, which becomes synonymous with $\tilde{n}_+=\tilde{n}_-\exp(i\varphi)$. The phase of $\tilde{I}_+$ and $\tilde{I}_-$ is almost in phase in very low frequency, for instance, at $\omega/2\pi=0.1$ kHz in Fig. 7(a). The phase starts to become out of phase with increasing $\omega/2\pi$. The phase is in phase again at $\omega/2\pi=10$ kHz as shown in Fig. 7(b). The phase becomes finally constant with phase inversion independently of $\omega/2\pi$ in high frequency, as seen at $\omega/2\pi=20$ kHz in Fig. 7(c). As a detailed expression of the frequency dependence of φ, a phase-lag spectrum is shown in Fig. 8, where closed and open circles denote the phase-lag spectrum and the measured dispersion relation the same as Fig. 6, respectively. φ drastically changes for variations in $\omega/2\pi$ below 15 kHz. The phase lag largely increases

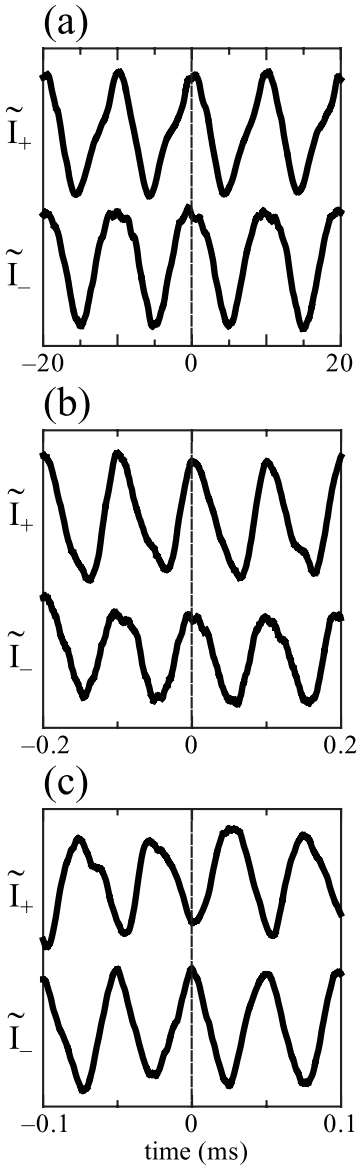

FIG. 7. Temporal variations of the positive- and negative-saturation currents, $\tilde{I}_+$ and $\tilde{I}_-$, for $\omega/2\pi$=(a) 0.1, (b) 10, and (c) 20 kHz at r=0 cm and z=5 cm.

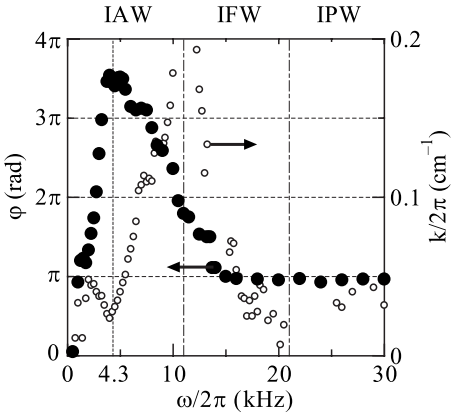

FIG. 8. Phase lag φ between $\tilde{I}_+$ and $\tilde{I}_-$ is defined as $\tilde{I}_+ = \tilde{I}_- \exp(i\varphi)$. The phase-lag spectrum shown by closed circles and the dispersion relation by open circles which is the same in Fig. 6.

in proportion to $\omega/2\pi$ in the low-frequency range of IAW ($\omega/2\pi < \omega_c/2\pi$). It was shown in the previous result that the phase lag greatly changes in the low-frequency range, but the details of the dispersion relation and the phase lag at around $\omega_c/2\pi$ could not be measured. The improvement of the exciter structure and the relevant applied voltage V_{cy} enables us to measure the branch separation and the phase-lag change of IAW in detail. The phase lag becomes $\varphi = 7\pi/2$ at $\omega_c/2\pi$ and the phase lag inversely decreases in proportion to $\omega/2\pi$ in $\omega_c/2\pi < \omega/2\pi < 15$ kHz. The phase lags of IFW and IPW in $\omega/2\pi > 15$ kHz are π independently of $\omega/2\pi$. The φ property of IAW in the pair-ion plasma is unique, because the phase lag between the electron and ion densities in ordinary electron-ion plasmas usually has little change. The backwardlike mode joining the two branches of IAW is apparently analogous to IFW in the dispersion relation, but the φ property is quite different, that is, the backwardlike mode has a strong frequency dependence of φ, but IFW does not. The phase lags of IFW and IPW are reversed, which means that a charge separation is realized and electrostatic-potential structures are formed in the pair-ion plasma in the dynamical state. This is in contrast to the measured result that the electrostatic-potential structures including sheaths are almost not formed in the stationary state. In ordinary electron-ion plasmas, φ is close to zero for IAW and φ cannot be defined for the electron plasma wave (synonymous with IPW in the pair-ion plasma) because the ion response is very slow compared with the electron response and the ion-density fluctuation is ignored. Thus, IFW and IPW with $\varphi \simeq \pi$ reflects a special situation.

In addition to the above-mentioned properties of the modes propagating along the B-field lines at r=0 cm, a surface structure of longitudinal waves is investigated by measuring a temporal variation of the radial-plasma profile. Typical radial wave patterns at z=5 cm are shown at $\omega/2\pi$=(a), 1.5 (b) 10, (c) 19, and (d) 40 kHz in Fig. 9, where the fluctuation component is $\tilde{I}_+$. The radial wave front is almost uniform, while the phase in the periphery is slightly delayed in comparison with that in the center at $\omega/2\pi$=40 kHz (IPW). The amplitude becomes maximum at r=0 cm and is proportional to the time-averaged density. The amplitude profiles are almost Gaussian, thus, IAW, IFW, and IPW seem to be plane waves.

The cylindrical exciter has been used for the excitation of the modes. The electric field of the exciter neighborhood ($|r| \sim 2.4$ cm) is strong in the cross section of the exciter. The periphery ($|r| > 2.6$ cm) of the plasma is a diffusion region with low density and considered to be in vacuum. Surface waves propagating along the B-field lines are theoretically predicted to be excited at around the boundary between the plasma and the vacuum regions. If the surface waves were excited, its maximum amplitude would be localized at around the boundary, but the radial-amplitude profiles of the modes are Gaussian. Therefore, it can be said that the excited modes are not surface waves. Since the cylindrical exciter inevitably yields the inhomogeneous structure of the radial-electric-field profiles, this exciter is not necessarily suitable

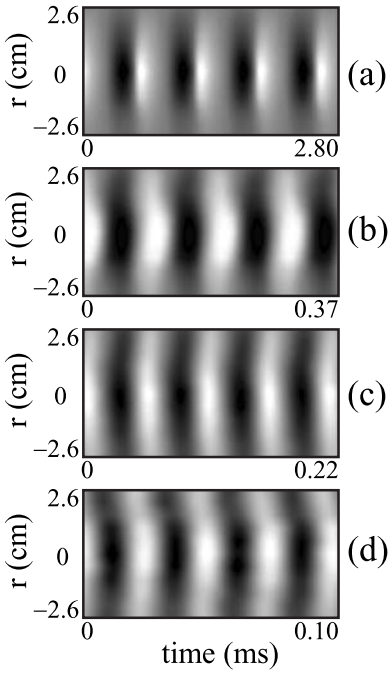

FIG. 9. Radial wave patterns of IAW, IFW, and IPW for $\omega/2\pi$=(a) 1.5, (b) 10, (c) 19, and (d) 40 kHz at z=5 cm.

for the plane-wave excitation, and so the cylindrical exciter is changed to a grid exciter, as shown in Fig. 10. In our previous works, when a grid electrode was inserted into the plasma cross section, serious problems were caused that the density in region (III) becomes lower and an insulating thin film of C_{60} is formed on the surface of the grid made of a stainless steel. When the insulating film covers the grid surface, the electric field is not applied to the plasma and the modes cannot be excited. Thus, the grid exciter has not been used in the pair-ion plasma until now, although the mode excitation using the grid exciter has been a standard technique in ordinary-plasma experiments. Since we experimentally find a fact that the use of a copper grid and its retention temperature higher than 400 °C evade the adherence of C_{60} on the grid surface, the modes can be excited by the grid exciter now. The dispersion relation of the propagating modes excited by the grid exciter is shown in Fig. 11, where both IAW and IFW are focused. Closed and open circles denote the dispersion relations obtained from the grid and the cylindrical excitations, respectively. The both dispersion relations almost accords in $\omega/2\pi > \omega_c/2\pi$=4.3 kHz. In the case of grid excitation, however, the backwardlike mode is observed more clearly in $2.5 < \omega/2\pi < 4.3$ kHz, and the clear-cut division of IAW into two branches is resultantly seen in $\omega/2\pi < 2.5$ kHz and $4.3 < \omega/2\pi < 12$ kHz. The branches propagating obliquely are theoretically predicted. In the experiment, the branches appear to propagate almost along the B-field lines, but they might include the wave-number component in the radial direction, which is discussed in Sec. IV. The backwardlike mode is not predicted theoretically at this time.

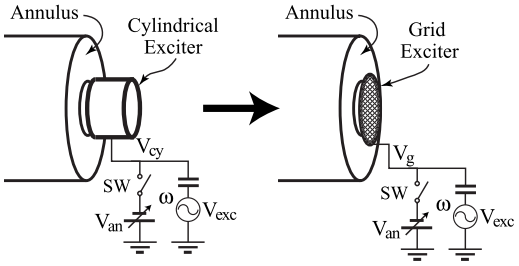

FIG. 10. The cylindrical exciter is changed to a grid exciter. Both the exciters are made by copper for prevention of adhesion of C_{60}.

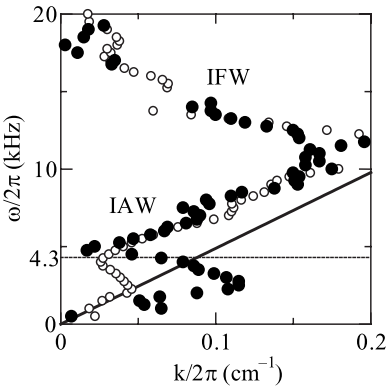

FIG. 11. Dispersion relations of modes excited by cylindrical (open circles) and grid (closed circles) exciters. Solid curve denotes the calculated relation, the same as Fig. 6.

IV. DISCUSSION

Some theoretical works have already been presented, which concern linear and nonlinear collective modes in nonrelativistic electron-positron plasmas [4,5,7,10–12,14,15]. A comprehensive two-fluid model has been developed for collective-mode analyses, based on which longitudinal and/or transverse electrostatic and/or electromagnetic modes have been studied. The longitudinal collective modes are analogous to those in ordinary electron-ion plasmas. On the other hand, the transverse collective modes in the presence of a magnetic field are different from those in the ordinary plasmas, for instance, the whistler mode does not exist. Here, electrostatic modes are focused in the pair-ion plasma, because the density and the temperature are relatively low and the induction current of the ions is very small, and electromagnetic modes relevant to the plasma can be neglected in our experiment.

The two fluid equations in the absence of the B field appropriate to the pair-ion plasma consist of the usual momentum and continuity equations for each ion species, supplemented by Poisson's equation:

$$mn_j\left(\frac{\partial v_j}{\partial t} + (v_j \cdot \nabla)v_j\right) = -q_j n_j \nabla \phi - \gamma T_j \nabla n_j, \qquad (1)$$

$$\frac{\partial n_j}{\partial t} + \nabla \cdot (n_j v_j) = 0, \qquad (2)$$

$$\nabla^2\phi = -\frac{e}{\varepsilon_0}(n_+ - n_-), \tag{3}$$

where m, n_j, v_j, q_j, T_j, and ϕ denote the mass, the density, the fluid velocity, the charge, the temperature, and the potential, respectively. The subscript j denotes positive or negative ions, $j=+$ or $-$, respectively. γ is the ratio of specific heats C_p/C_v and ε_0 is the permittivity of free space. The dispersion relations are linearized for a homogeneous unbounded plasma (ion temperatures $T=T_+=T_-$), and the phase lag φ is defined as $\tilde{n}_+=\tilde{n}_-\exp(i\varphi)$ described in Sec. III B, the coupled linear mode equations are derived

$$\omega^2 - c_s^2k^2 - [1-\exp(-i\varphi)]\omega_p^2 = 0, \tag{4}$$

$$\omega^2 - c_s^2k^2 - [1-\exp(i\varphi)]\omega_p^2 = 0, \tag{5}$$

where the acoustic speed $c_s^2=\gamma T/m$ and the plasma frequency $\omega_p^2=e^2n_0/\varepsilon_0 m$ are introduced (n_0: plasma density). The dispersion relations associated with Eqs. (4) and (5) are simply given by

$$\omega^2 = c_s^2k^2 \quad (\varphi=0), \tag{6}$$

$$\omega^2 = c_s^2k^2 + 2\omega_p^2 \quad (\varphi=\pi). \tag{7}$$

The dispersion relations (6) and (7) give modes that correspond to an ion acoustic wave and an ion plasma wave in the pair-ion plasma, respectively. The dispersion relation corresponding to IFW cannot be derived in the simple two-fluid model. In general the ion temperature obtained from the Langmuir-probe characteristics is evaluated under the assumption that the velocity distribution functions of the ions are Maxwellian. But the distribution functions in the pair-ion plasma are likely half-Maxwellian because the ions passing through the annular hole flow downstream without being reflected by potential structures under the collisionless condition. Thus, the distribution function is defined as $f(v)=2n\sqrt{m/2\pi T}\exp(-mv^2/2T)$ $(v>0)$, where the thermal velocity is given by $v_{th}=\sqrt{T/m}$ in the case of $-\infty<v<\infty$. In this case, the drift velocity is calculated to be $v_d=\int_0^\infty vf(v)dv/\int_0^\infty f(v)dv=\sqrt{2T/\pi m}$. The effective thermal velocity is $v'_{th}=\int_0^\infty(v-v_d)^2f(v)dv/\int_0^\infty f(v)dv=\sqrt{(1-2/\pi)T/m}$, i.e., the effective temperature is $T'=(1-2/\pi)T$. The acoustic speed is $c_s=\sqrt{\gamma(1-2/\pi)T/m}=2.7\times10^4$ cm/s $(T=0.5$ eV). Therefore the phase-velocity comparison between the experiment and the theory requires making corrections to allow for this Doppler shift and the effective temperature (c_s+v_d). The dispersion curves of Eqs. (6) and (7) in consideration of the Doppler shift have been already shown in Figs. 6 and 11 in Sec. III B, which were calculated for $\gamma=3$ $[\gamma=(2+N)/N$, one-dimensional compression $N=1]$, $T=0.5$ eV (isotropy), and $n_0=1\times10^7$ cm^{-3}.

In the presence of a dc B field without magnetic fluctuations, the dispersion relations [14] are given by

$$\omega^2(\omega^2 - c_s^2k^2 - \omega_c^2) + c_s^2\omega_c^2k^2\cos^2\alpha = 0, \tag{8}$$

$$(\omega^2 - \omega_p^2)(\omega^2 - c_s^2k^2 - \omega_h^2) + c_s^2\omega_c^2k^2\cos^2\alpha = 0. \tag{9}$$

α is a propagation angle to the B-field lines and these modes at $\alpha=0$ are quite the same as those in the absence of the B field, except for the cyclotron oscillation ω_c and the upper hybrid oscillation $\omega_h=\sqrt{2\omega_p^2+\omega_c^2}$. The dispersion relations (8) and (9) give modes that correspond to acoustic and/or cyclotron waves and plasma and/or upper-hybrid waves in the ordinary plasmas, respectively.

The derived dispersion curves are compared with the measured dispersion relation in Fig. 6. Concerning the IAW property, since IAW divides into two branches at around the ion cyclotron frequency, the measured relation relatively fits the dispersion curve of Eq. (8), where the mode obliquely propagates. But the mode is measured to propagate almost along the B-field lines and the radial wave front is almost uniform in $z>4$ cm. The phase lag only in very low-frequency range $(\omega/2\pi<1$ kHz) is consistent with the theoretical prospects of Eq. (6). On the other hand, the phase lag of IAW in $1<\omega/2\pi<12$ kHz strongly depends on the frequency. The very existence of the backwardlike mode and IFW cannot be derived in these theoretical formulations. Concerning the IPW property, IPW measured relatively fits to the calculated curve in the previous result [45,47], but IPW considerably differs from the calculated one in Fig. 6. The phase lag of IPW is $\varphi=\pi$ as theoretically expected in Eq. (7) and the frequency dependence of φ does not appear. The pair-ion plasma frequency is estimated to be $\sqrt{2}\omega_p/2\pi \simeq 20$ kHz from the measured dispersion relation and the plasma density is calculated to be 3.3×10^6 cm^{-3}. This density is lower than that estimated from the probe measurement. Here, the phase difference between V_{cy} and I_+ at a frequency are labeled as θ_4, θ_5, and θ_6 at $z=4$, 5, and 6 cm, respectively. The wave number propagating along the B-field lines is obtained from these averaged values of $(\theta_5-\theta_4)/2\pi$ and $(\theta_6-\theta_5)/2\pi$ cm^{-1}. Thus, it cannot be denied the possibility that the other modes excited in the vicinity of the exciter affect the θ measurement. And the interference between IAW and IPW does not appear in the ordinary plasmas because the frequency bands of them are widely different, but IFW appears in the pair-ion plasma. This situation is the same as the backwardlike mode in $2.5<\omega/2\pi<4.3$ kHz. Thus, these modes are considered to be caused by the transition from one mode to another mode with close frequency. Properties of not only linear electrostatic waves but also nonlinear waves and electromagnetic waves in pair plasmas have been investigated in theory and simulation [49–64], but theoretical identification of them seems to have not been attained at present.

V. CONCLUSIONS

The generation of a pair-ion plasma, consisting of positive and negative ions of equal mass without electrons, is performed using a hollow electron beam in the presence of a uniform magnetic field, where electron-impact ionization and electron attachment play a key role. C_{60} of a stable cage is used as an ion source because it is easily charged positively (C_{60}^+) and negatively (C_{60}^-). A magnetic-filtering effect is

used for the separation of electrons and the ions. In the pair-ion plasma, static potential structures including sheaths are not almost formed. The active excitation of density modulation using a cylinder and/or grid exciter reveals the properties of electrostatic modes propagating along the magnetic-field lines. The modes are an ion acoustic wave (IAW) dividing into two branches at around the ion cyclotron frequency, a backwardlike mode joining the two branches, an ion plasma wave (IPW), and an intermediate-frequency wave (IFW) joining IAW and IPW. Phase lags between the density fluctuations of positive and negative ions for IAW and the backwardlike mode strongly depend on the frequency, but the phase lags for IPW and IFW are almost constant at π, which means that a charge separation is dynamically realized and dynamical potential structures are formed. These are unique phenomena which never appear in ordinary electron-ion plasmas.

ACKNOWLEDGMENTS

The authors would like to thank N. Tomioka, M. Musashi (Kobayashi), D. Date, and H. Iwata for their collaboration. This work was supported by a Grant-in-Aid for Scientific Research from the Ministry of Education, Culture, Sports, Science, and Technology, Japan.

[1] A. B. Mikhailovskii, O. G. Onishchenko, and E. G. Tatarinov, Plasma Phys. Controlled Fusion **27**, 527 (1985).
[2] N. Iwamoto, Phys. Rev. A **39**, 4076 (1989).
[3] U. A. Mofiz, Phys. Rev. A **40**, 2203 (1989).
[4] G. A. Stewart and E. W. Laing, J. Plasma Phys. **47**, 295 (1992).
[5] M. W. Sincell and J. H. Krolik, Phys. Fluids B **4**, 2669 (1992).
[6] V. I. Berezhiani, D. D. Tskhakaya, and P. K. Shukla, Phys. Rev. A **46**, 6608 (1992).
[7] N. Iwamoto, Phys. Rev. E **47**, 604 (1993).
[8] U. A. Mofiz and A. A. Mamun, Phys. Fluids B **5**, 1667 (1993).
[9] V. I. Berezhiani, V. Skarka, and S. Mahajan, Phys. Rev. E **48**, R3252 (1993).
[10] J. Zhao, K. I. Nishikawa, J. I. Sakai, and T. Neubert, Phys. Plasmas **1**, 103 (1994).
[11] G. A. Stewart, J. Plasma Phys. **50**, 521 (1993).
[12] S. Y. Abdul-Rassak and E. W. Laing, J. Plasma Phys. **50**, 125 (1993).
[13] J. Zhao, J. I. Sakai, K.-I. Nishikawa, and T. Neubert, Phys. Plasmas **1**, 4114 (1994).
[14] G. P. Zank and R. G. Greaves, Phys. Rev. E **51**, 6079 (1995).
[15] J. Zhao, J. I. Sakai, and K.-I. Nishikawa, Phys. Plasmas **3**, 844 (1996).
[16] A. D. Rogava, S. M. Mahajan, and V. I. Berezhiani, Phys. Plasmas **3**, 3545 (1996).
[17] D. H. E. Dubin, Phys. Rev. Lett. **92**, 195002 (2004).
[18] G. Gibson, W. C. Jordan, and E. J. Lauer, Phys. Rev. Lett. **5**, 141 (1960).
[19] C. M. Surko, M. Leventhal, and A. Passner, Phys. Rev. Lett. **62**, 901 (1989).
[20] C. M. Surko and T. J. Murphy, Phys. Fluids B **2**, 1372 (1990).
[21] R. G. Greaves, M. D. Tinkle, and C. M. Surko, Phys. Plasmas **1**, 1439 (1994).
[22] M. D. Tinkle, R. G. Greaves, and C. M. Surko, Phys. Plasmas **2**, 2880 (1995).
[23] H. Boehmer, M. Adams, and N. Rynn, Phys. Plasmas **2**, 4369 (1995).
[24] R. G. Greaves and C. M. Surko, Phys. Plasmas **4**, 1528 (1997).
[25] E. P. Liang, S. C. Wilks, and M. Tabak, Phys. Rev. Lett. **81**, 4887 (1998).
[26] R. G. Greaves and C. M. Surko, Phys. Plasmas **8**, 1879 (2001).
[27] C. Gahn, G. D. Tsakiris, G. Pretzler, K. J. Witte, P. Thirolf, D. Habs, C. Delfin, and C.-G. Wahlström, Phys. Plasmas **9**, 987 (2002).
[28] M. Amoretti *et al.*, Phys. Rev. Lett. **91**, 055001 (2003).
[29] N. Sato, T. Mieno, T. Hirata, Y. Yagi, R. Hatakeyama, and S. Iizuka, Phys. Plasmas **1**, 3480 (1994).
[30] W. Oohara, S. Ishiguro, R. Hatakeyama, and N. Sato, J. Phys. Soc. Jpn. **71**, 373 (2002).
[31] W. Oohara, R. Hatakeyama, and S. Ishiguro, Plasma Phys. Controlled Fusion **44**, 1299 (2002).
[32] W. Oohara, R. Hatakeyama, and S. Ishiguro, Phys. Rev. E **68**, 066407 (2003).
[33] M. Lezius, P. Scheier, and T. D. Märk, Chem. Phys. Lett. **203**, 232 (1993).
[34] T. Jaffke, E. Illenberger, M. Lezius, S. Matejcik, D. Smith, and T. D. Märk, Chem. Phys. Lett. **226**, 213 (1994).
[35] J. Huang, H. S. Carman, Jr., and R. N. Compton, J. Phys. Chem. **99**, 1719 (1995).
[36] H. Deutsch, K. Becker, J. Pittner, V. Bonacic-Koutecky, S. Matt, and T. D. Märk, J. Phys. B **29**, 5175 (1996).
[37] Y. V. Vasil'ev, R. F. Tuktarov, and V. A. Mazunov, Rapid Commun. Mass Spectrom. **11**, 757 (1997).
[38] O. Elhamidi, J. Pommier, and R. Abouaf, J. Phys. B **30**, 4633 (1997).
[39] R. Völpel, G. Hofmann, M. Steidl, M. Stenke, M. Schlapp, R. Trassl, and E. Salzborn, Phys. Rev. Lett. **71**, 3439 (1993).
[40] S. Matt, B. Dünser, M. Lezius, H. Deutsch, K. Becker, A. Stamatovic, P. Scheier, and T. D. Märk, J. Chem. Phys. **105**, 1880 (1996).
[41] V. Foltin, M. Foltin, S. Matt, P. Scheier, K. Becker, H. Deutsch, and T. D. Märk, Chem. Phys. Lett. **289**, 181 (1998).
[42] D. Hathiramani, P. Scheier, K. Aichele, W. Arnold, K. Huber, and E. Salzborn, Chem. Phys. Lett. **319**, 13 (2000).
[43] A. A. Vostrikov, D. Yu. Dubnov, and A. A. Agarkov, High Temp. **39**, 22 (2001).
[44] W. Oohara and R. Hatakeyama, Phys. Rev. Lett. **91**, 205005 (2003).
[45] R. Hatakeyama and W. Oohara, Phys. Scr., T **T 116**, 101 (2005).
[46] W. Oohara, Y. Kuwabara, and R. Hatakeyama, in *New Vistas in Physics of Dusty Plasmas: Fourth International Conference on*

the Physics of Dusty Plasmas, edited by L. Boufendi *et al.*, AIP Conf. Proc. No. 799 (AIP, Melville, NY, 2005), p. 29.
[47] W. Oohara, D. Date, and R. Hatakeyama, Phys. Rev. Lett. **95**, 175003 (2005).
[48] D. P. Sheehan and N. Rynn, Rev. Sci. Instrum. **59**, 1369 (1988).
[49] P. K. Shukla, Phys. Scr., T **113**, 7 (2004).
[50] P. K. Shukla and M. Khan, Phys. Plasmas **12**, 014504 (2005).
[51] A. Hasegawa and P. K. Shukla, Phys. Scr., T **116**, 105 (2005).
[52] F. Verheest and T. Cattaert, Phys. Plasmas **12**, 032304 (2005).
[53] H. Schamel and A. Luque, New J. Phys. **7**, 69 (2005).
[54] P. K. Shukla and L. Stenflo, Phys. Plasmas **12**, 044503 (2005).
[55] B. Eliasson and P. K. Shukla, Phys. Rev. E **71**, 046402 (2005).
[56] F. Verheest and G. S. Lakhina, New J. Phys. **7**, 94 (2005).
[57] J. Vranjes and S. Poedts, Plasma Sources Sci. Technol. **14**, 485 (2005).
[58] F. Verheest, Nonlinear Processes Geophys. **12**, 569 (2005).
[59] A. Luque, H. Schamel, B. Eliasson, and P. K. Shukla, Phys. Plasmas **12**, 122307 (2005).
[60] H. Saleem, J. Vranjes, and S. Poedts, Phys. Lett. A **350**, 375 (2006).
[61] A. Luque, H. Schamel, B. Eliasson, and P. K. Shukla, Plasma Phys. Controlled Fusion **48**, L57 (2006).
[62] Z. Jian, Chin. Phys. **15**, 1028 (2006).
[63] H. Saleem, Phys. Plasmas **13**, 044502 (2006).
[64] I. Kourakis, A. Esfandyari-Kalejahi, M. Mehdipoor, and P. K. Shukla, Phys. Plasmas **13**, 052117 (2006).